Special topic

Sara Linse*

Mechanism of amyloid protein aggregation and the role of inhibitors

https://doi.org/10.1515/pac-2018-1017

Abstract: Inhibition of amyloid β peptide (Aβ) aggregation is an important goal due to the connection of this process with Alzheimer's disease. Traditionally, inhibitors were developed with an aim to retard the overall macroscopic aggregation. However, recent advances imply that approaches based on mechanistic insights may be more powerful. In such approaches, the microscopic steps underlying the aggregation process are identified, and it is established which of these step(s) lead to neurotoxicity. Inhibitors are then derived to specifically target steps involved in toxicity. The Aβ aggregation process is composed of at minimum three microscopic steps: primary nucleation of monomers only, secondary nucleation of monomers on fibril surface, and elongation of fibrils by monomer addition. The vast majority of toxic species are generated from the secondary nucleation process: this may be a key process to inhibit in order to limit toxicity. Inhibition of primary nucleation, which delays the emergence of toxic species without affecting their total concentration, may also be effective. Inhibition of elongation may instead increase the toxicity over time. Here we briefly review findings regarding secondary nucleation of Aβ, its dominance over primary nucleation, and attempts to derive inhibitors that specifically target secondary nucleation with an aim to limit toxicity.

Keywords: aggregation mechanism; Distinguished Women in Chemistry and Chemical Engineering; inhibitor design; self-assembly.

Introduction

Nucleation of amyloid β peptide (Aβ) aggregates on the surfaces of Aβ fibrils has emerged in the past decade as a major pathway for the generation of molecular species responsible for cellular toxicity and autocatalytic proliferation of fibrillar aggregates [1–4]. Primary nucleation involves monomers only, and may occur in bulk (Fig. 1a) or on a foreign surface (Fig. 1b). Monomer-dependent secondary nucleation is defined as a process whereby nucleus formation from monomers is catalyzed by aggregates composed of the same type of monomeric building blocks (Fig. 1c). The monomers thus form a nucleus on the surface of an already existing aggregate (Fig. 1c). By definition, secondary nucleation happens in the presence of a parent seed aggregate of the same kind of monomers. Secondary nucleation is thus not the same as heterogeneous primary nucleation (Fig. 1b), which happens in the vicinity of foreign surfaces of for example phosholipid membranes [5], nanoparticles [6, 7], at the air-water interface [8] or any surfaces present in the system. Both secondary nucleation and heterogeneous primary nucleation speed up the aggregation process, and thus share some similarities on an energetic level, although the effect on the macroscopically observable kinetics curves may not be the same. The molecular mechanisms of the two nucleation processes and the catalytic roles of the surfaces are probably different. Both surfaces may provide "binding sites", or merely surface accumulation of monomers, whereby increased local concentration of monomers may govern nucleation. However, only the aggregate of the same kind of monomers has a structure that the forming nucleus can

***Corresponding author: Sara Linse,** Lund University, Department of Biochemistry and Structural Biology, P.O. Box 124, 221 00 Lund, Sweden; and Lund University, NanoLund, Lund, Sweden, e-mail: sara.linse@biochemistry.lu.se

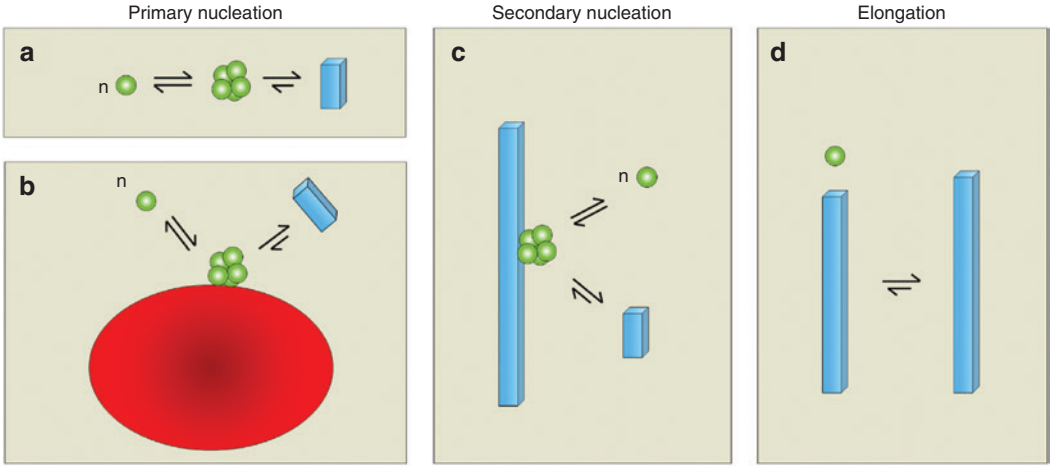

Fig. 1: Primary nucleation, secondary nucleation and elongation. Primary nucleation involves monomers of one substance in solution (a), or on the surface of a foreign object, heterogeneous primary nucleation (b). Secondary nucleation involves monomers of one substance on the surface of an already existing aggregate of the same substance (c). Elongation occurs by monomer addition to the ends of fibrils (d). Green spheres symbolize monomers, but does not refer to their structure which is more or less extended in cases of amyloid peptides. Blue cuboids symbolize amyloid fibrils.

copy and that the new aggregate can take up. Only secondary nucleation can lead to autocatalytic amplification of aggregate mass.

Several devastating human diseases are linked to amyloid formation of a defined set of proteins [9–14]. The close connection with neurodegenerative conditions such as Alzheimer's and Parkinson's diseases motivates detailed studies of secondary nucleation of amyloid formation. The goal of these studies is to unravel the molecular determinants of secondary nucleation, including enhancing and attenuating factors, as well as its underlying mechanism and composite molecular steps. These composite steps may include arrival at the fibrils surface, product formation and release (Fig. 1c). A number of scenarios are possible as to the detailed sequence of events and structural features involved (Fig. 2) and it is also possible that multiple such pathways co-exist. Defining the molecular requirements for secondary nucleation, and its generation of neurotoxic species, will facilitate the design and search for potent secondary nucleation inhibitors. This will make it possible to interfere with secondary nucleation and limit toxicity. The analogy with secondary nucleation processes in many other self-assembling systems, implies that it may be possible to reach a general physicochemical understanding of the process. There is for example a long history of literature on industrial crystallization methods, where control over secondary nucleation is key to deriving products with well-defined structure and function (for review see Ref. [15]). Taking control over secondary nucleation of amyloid-forming peptides may aid both in therapeutic intervention in amyloid diseases and in forming distinct products with unique materials properties.

Monomer-dependent secondary nucleation of Aβ was reported as late as 2013, although this key microscopic step was established in many systems since the start of the 1900s [15–18]. There are many examples of 3D assembly formation processes for which secondary nucleation has been found to accelerate the propagation of aggregates with the same structure as the parent seed. This includes for example crystallization of proteins and small molecules [19–24] formation of nanoparticles [25, 26], zeolites [27], and other assemblies of inorganic and organic compounds [15, 28, 29]. In addition to experimental observations, secondary nucleation has been inferred from molecular dynamics simulations of the crystallization of Lennard-Jones particles to depend on the relative strength of solvent-solvent, solute-solute and solvent-solute interactions [24]. In terms of protein aggregation processes, secondary nucleation of protein monomers on the surface of existing protein fibers was established in the 1980s for the formation of actin filaments and the fibrous aggregates of sickle cell hemoglobin [30–32]. Secondary nucleation is reported to be enantio-specific [19], and has been suggested to explain prion propagation [33].

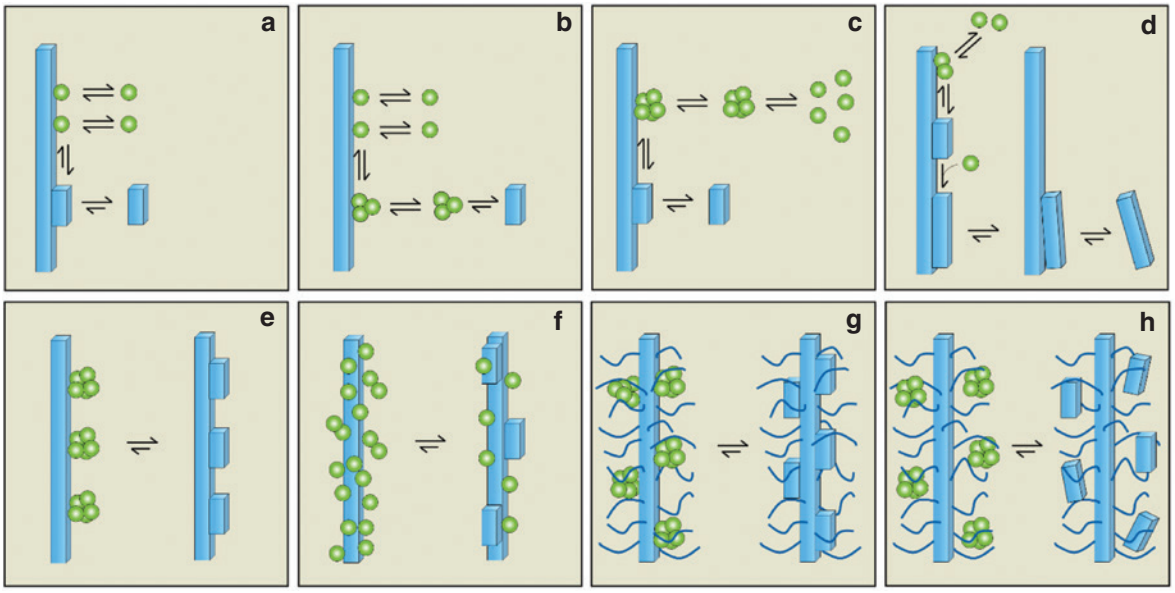

Fig. 2: Secondary nucleation of monomers on fibril surface – cartoons of possible scenarios. Monomers of one substance may nucleate in solution (primary nucleation, left) or on the surface of an already existing aggregate (secondary nucleation, right). Green and blue color symbolize the conformation in free state and aggregated state, respectively.

Some commonly used definitions of nuclei, oligomers and seeds

Very small clusters of monomers have a high interfacial energy towards water and hence a high free energy per monomer; as a consequence, they have a high probability to dissociate into their component monomers. A critical nucleus is often defined as the smallest aggregate which grows faster by monomer addition than it dissociates back to smaller aggregates and monomers. Oligomers is a wider definition and includes many kinds of assemblies containing more than one monomer. The definition of oligomers may be operational. i.e. including all aggregated species eluting in a certain range of volumes from a size exclusion column, all aggregates that grow more slowly than fibrils, all aggregates that have a different structure than fibrils, all aggregates that are more toxic than fibrils, or it may be defined as all aggregates within a defined size range, e.g. 2–30 mers irrespective of their structure. Oligomers can be formed both by primary and secondary nucleation processes. However, once a critical concentration of Aβ fibrils are formed by primary nucleation, i.e. over the major part of the reaction time-course, secondary nucleation is the process that most rapidly increases the number of oligomers. The term "fibrillar oligomers" might be used to refer to oligomers that have converted to fibrillar structure but are transiently much shorter than the fibrils present at equilibrium. The term seed is typically used for fibrils that are added to a supersaturated monomer solution; this leads to rapid generation of new fibrils with the same morphology, chirality and local packing of monomers as in the seed [19]. The seed fibrils may collected at the end of a quiescent reaction, and used as is, or if the goal of the seeding experiment is to study the relative rates of elongation and secondary nucleation, then the fibrils may also be mechanically broken before use to increase the number of ends per fibril length. Seeds can have an operational definition and may then include all species that speed up the aggregation of monomers compared to monomers alone at the same concentration.

Amyloid formation mechanisms are challenging to study

It is relevant to ask why the understanding of amyloid protein aggregation mechanisms is lagging behind the understanding of several other self-assembling systems as mentioned above. Amyloid proteins are for many

reasons challenging to study, and some early investigations suffered form large sample-to-sample variations in the observed kinetics data, which made detailed mechanistic analysis impossible. A bottle-neck was the difficulties in early work to obtain the amyloid proteins in sequence homogeneous and pure form. Moreover, many amyloid proteins display very slow homogeneous primary nucleation, and are therefore highly sensitive to any variation in solution conditions as well as to any variation in the area and character of all surfaces of the systems under study [7], including those of the sample containers a well as the air-water-interface [8]. Another reason for the relatively slow development might be that, in part, the amyloid field was hypothesis driven – mechanism were postulated and published, and experiments were then designed to prove or disprove mechanisms, one-by-one. We argue that a faster route might be to apply a more unbiased chemical kinetics approach.

A chemical kinetics approach

A chemical kinetics approach [34] operates as follows. First, methodology is established to (i) obtain the protein or peptide of interest in sequence homogeneous and ultra-pure form, (ii) produce supersaturated solutions of isolated monomer, and (iii) take control over solution conditions as well as the inertness and area of all surfaces present in the experimental system. Second, a wealth of data of aggregate mass versus time is collected for initially supersaturated samples at a range of monomer concentrations. Third, models of increasing complexity are fitted to all data globally, and the minimal model that can reproduce all data satisfactorily is chosen [35]. Fourth, the chosen model is used to predict the outcome of new experiments with altered starting conditions. These experiments are conducted and the model is either validated or discarded, and a more complex model may be needed to explain all data. The model obtained using such an approach represents a mechanism that is compatible with all data; however, one can never exclude the possibility that there is some other mechanism and model that could possibly fit all data, or that the model used is an over-simplification.

A chemical kinetics approach to Aβ42 aggregation

Aβ42 is a surface-active peptide with amphiphatic sequence (Fig. 3), and was colloquially known as “the peptide from hell” [37] because failure to purify and handle Aβ42 had lead to irreproducible results and hampered quantitative analysis. Application of a chemical kinetics approach to Aβ42 was thus a formidable challenge and required an optimization of the whole work-flow for the kinetic experiment. Recombinant peptide was chosen because of the much superior fidelity of translation at the ribosome compared to chemical peptide synthesis. Expression provides a homogeneous sequence and avoids the high cost, high error frequency and batch-to-batch variation of synthetic peptides, factors that distort the kinetics [38]. Expression “as is” with no tags, except the starting Met residue that precedes Asp1, made it possible to design an affordable purification protocol based on scalable procedures such as ion exchange and size exclusion chromatography [39]. Critical to the experimental setup, ultra-pure peptide was isolated in monomeric form and stored at –20 °C as multiple identical aliquots, and monomers were again isolated by gel filtration just prior to starting the aggregation kinetics. Each chromatographic step may lead to large (up to 50 %) losses of peptide; however, the additional gel filtration step is absolutely key to obtaining results that are reproducible between repeats of the experiment and over peptide batches. Other key considerations in the experimental setup includes the extensive degassing of buffers, optimization of the concentration of the reporter dye, thioflavin T (ThT), to an interval where its fluorescence signal is linearly dependent on the mass concentration of fibrils [1], and where its presence does not affect the formation kinetics [40], as well as choosing as small and inert as possible surfaces of the reaction containers. The use of half-area 96-well back polystyrene plates with PEG-coated surface is based on a QCMd study that failed to observe any interaction of Aβ with PEGylated

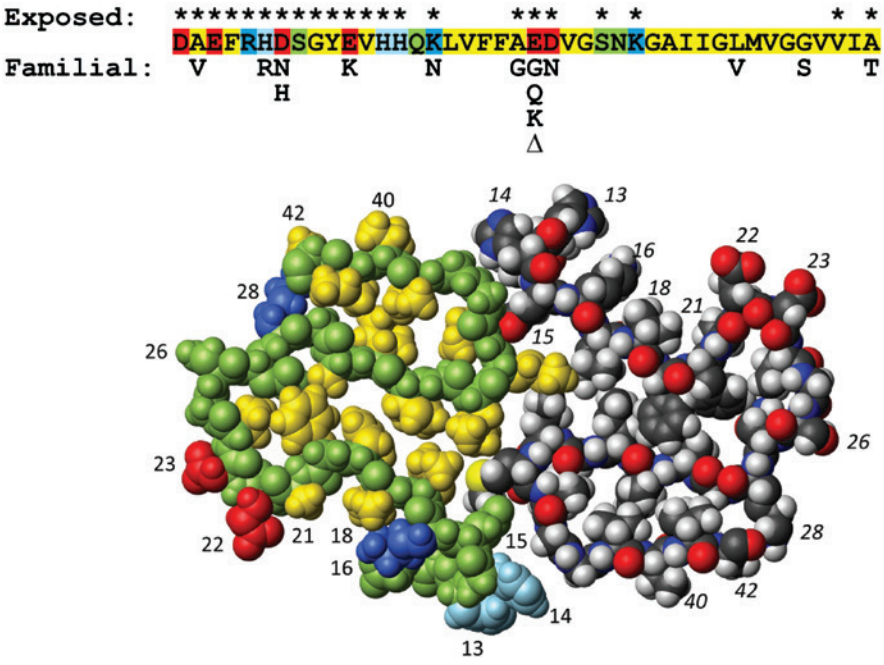

Fig. 3: Aβ42 sequence (top) and the Aβ42 fibril structure (bottom, 5KK3.pdb [36]), from which one plane with two monomers is shown. The sequence and sidechains in the left monomer are color coding according to amino acid residue character: negatively charged (red), positively (charged (blue), titrating around neural pH (light blue), hydrophilic (green) and hydrophobic (yellow). Tyr10 and Met35 where colored yellow although they have mixed polar/nonpolar character. Residues with exposed side chains in the fibril structure are marked with a star above the sequence and numbered in the structure. The right monomer in the fibril plane is shown with standard cpk coloring: carbon (dark gray), hydrogen (white), oxygen (red), nitrogen (blue) and sulfur (yellow). The Figure was prepared using Molmol [65].

surfaces, in contrast to most other surfaces [41]. Once all these factors are controlled, Aβ42 aggregates in a highly reproducible manner on precisely the same time-scale for every repeat with identical starting conditions [42]. This is expected in analogy with other self-assembling systems, for which highly pure macroscopic samples and controlled conditions lead to high reproducibility in reaction rates as well as the morphologies of the formed aggregates.

Secondary nucleation of Aβ42 – global analysis of non-seeded data

The chemical kinetics approach was applied to Aβ42 from Alzheimer's disease. The first set of experimental data included the concentration-dependent time course of amyloid fibril formation from solutions of Aβ42 monomers at a range of initial concentrations at quiescent conditions, 37 °C, 20 mM sodium phosphate buffer, 0.2 mM EDTA, 0.02 % (w/v) NaN_3, pH 8.0 [1]. The reaction was kick-started by a temperature jump from zero to 37 °C, and aggregation monitored using thioflavin T (ThT) fluorescence in a plate reader. We failed to fit the Aβ42 data using master equations describing primary nucleation and fibril growth processes only (Fig. 4a). Our data shows a lag phase followed by sharp, almost exponential, growth in the fibril mass, which was not captured by models lacking secondary nucleation pathways. Addition of a filament fragmentation step, as had explained a range of other data [43], resulted in steeper curves but also a weaker concentration dependence than what was observed and thus, did not lead to any improvement of the global fit to all curves (Fig. 4b). However, if secondary nucleation of monomers on the surface of fibrils [44–47] was added besides primary nucleation and elongation, it was possible to obtain reasonable global fits to all data points for the concentration-dependent aggregation kinetics (Fig. 4c).

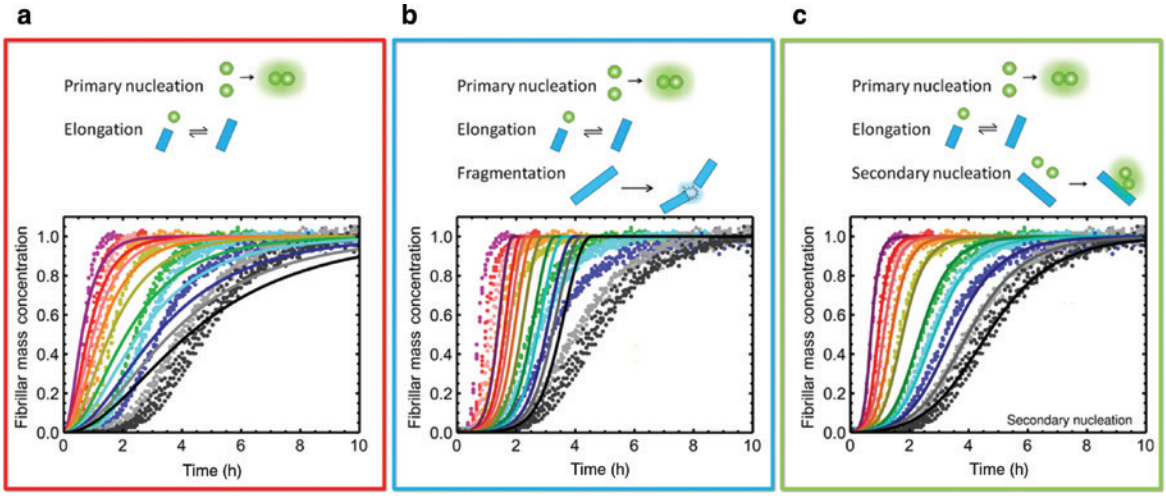

Fig. 4: Secondary nucleation improves global fit to Aβ42 aggregation kinetics data. (a–c) Fibril formation kinetics starting from monomer solutions at several concentrations (individual colors, each concentration in quadruplicate) in 20 mM NaP, 0.2 mM EDTA, 0.02 % NaN_3, pH 8.0. (a) Best fit of a model with primary nucleation and elongation. (b) Adding a fibril fragmentation step leads to sharper curves but also more narrow concentration dependence and cannot fit the data. (c) Best fit of a model with primary nucleation, elongation and secondary nucleation of monomers on aggregate surface. Data from Ref. [1].

In principle, all fibril-dependent processes that lead to increased number of aggregates may be called secondary nucleation. Thus in some literature, fragmentation is also called secondary nucleation. In a global kinetic analysis, monomer-dependent secondary nucleation can be distinguished from fragmentation based on the steepness of the transitions of individual curves in relation to the monomer-dependence of the transition mid-point (Fig. 4c vs. 4b, [1, 47]), although the difference between the two models is smaller in cases where monomer-dependent secondary nucleation saturates [2].

Seeded experiments confirm secondary nucleation of Aβ42

The global kinetic analysis (Fig. 4) provided initial evidence of the role of monomer-dependent secondary nucleation in Aβ42 aggregation. One key prediction was that the addition of small amounts of preformed fibrils (seeds) would bypass the primary nucleation process, resulting in almost all new fibrils being generated through secondary nucleation. Indeed, it was observed that the addition of a seed quantity so small that the sigmoidal-like shape of the growth curve is conserved, changed the timescale of the aggregation reaction to such an extent that the entirety of the peptide was converted into aggregates before the corresponding reaction in the absence of seeds had proceeded through the lag phase (Fig. 5, [1]). These data confirmed that the presence of a fibril-dependent nucleation process.

Isotope labeling identifies Aβ42 monomers as the origin of new aggregates during secondary nucleation

As a second set of validation, radio-isotope labeling was used to pinpoint the origin of the new aggregates that were generated in the presence of fibrils. One set of experiments employed radio-active monomer mixed with unlabeled seeds, and another set employed unlabeled monomer mixed with radioactive seeds. Both kinds of samples were incubated until half the monomers were converted to fibrils, the point in time where the oligomer concentration is close to its maximum. Fibrils were removed by centrifugation and the super-

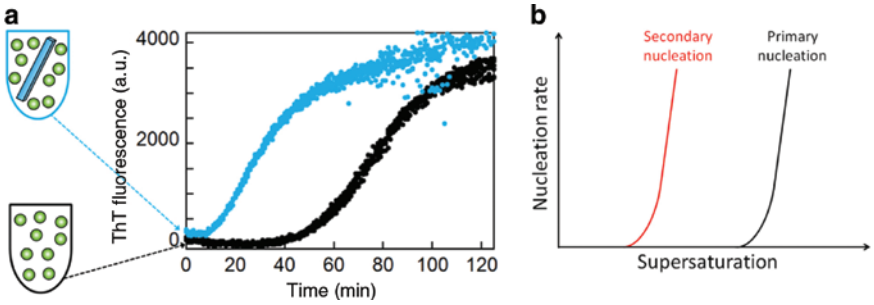

Fig. 5: Secondary nucleation shortens the lag phase already at low seed concentration. (a) Monomeric samples supplemented at time zero with a low (on the order of 1 %) concentration of seeds (blue) show reduced lag phase relative to non-seeded reactions starting at time zero from monomer only (black). This signifies a secondary, seed-dependent, process which catalyses the aggregation of the monomers. Data from Ref. [1]. (b) Primary (black) and secondary (red) nucleation rate as a function of supersaturation. Adapted from Ref. [61].

natant separated by size exclusion chromatography to remove monomers and isolate oligomers for radio-counting. By this procedure, oligomers become defined as aggregated species eluting between the void and the monomers, but without overlap with the monomer peak, i.e. ca. 3-mers to 20-mers. Radioactive oligomers were found to be formed in the sample where radioactive monomer had been mixed with unlabeled seeds, but not in the sample where unlabeled monomer had been mixed with radioactive seeds (Fig. 6). Thus, the new aggregates were generated from monomer in a fibril-catalyzed reaction, and not due to fragmentation of the fibrils. In summary, kinetic analysis indicated that the aggregation mechanism is dominated by a secondary pathway, while seeded experiments and the use of radioactive peptide showed that secondary nucleation produces new aggregates from monomer in the presence of fibrils [1].

Secondary nucleation of Aβ variants, α-syn and amylin

After monomer-dependent secondary nucleation was established for Aβ42 [1], it was found for Aβ40 [2], for N-terminally modified Aβ42 variants [48, 49] and for mutational variants leading to early onset Alzheimer's disease [50–52]. Another protein for which secondary nucleation is prominent is α-syn involved in Parkinson's disease. In this case, the mechanism of fibril propagation and growth is highly dependent on pH and at neutral pH the reaction is dominated by elongation of seeds [53]. Secondary nucleation occurs at mildly acidic pH, below pH 6.0, and was inferred from global fits to aggregation data, and confirmed using seeding experiments, as well as analyses of monomer-fibril interaction and size distribution [53, 54]. Secondary nucleation in amyloid formation has also been reported for insulin [55] and amylin [56] involved in diabetes.

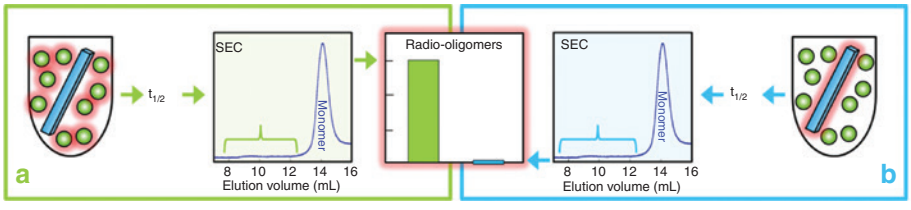

Fig. 6: Radio-assay with radioactive monomer and 1 % unlabeled seed (a) or unlabeled monomer and 1 % radioactive seed (b). Both samples were incubated until half the monomers had converted to fibrils, which were removed by centrifugation. The supernatant was subjected to size-exclusion chromatography to remove monomer and to collect the oligomer fractions. Radio-oligomers were detected for sample A (green bar) but not for sample B (blue bar). This shows that new aggregates (oligomers) are generated from monomer in a reaction catalyzed by the seed fibrils. For a reaction starting from 5 μM radioactive monomer ca. 75 nM radioactive oligomers were detected [1].

Connection between microscopic processes and macroscopic observations

Amyloid reactions are often studied by methods that monitor the concentration of monomers or fibrils as a function of time and thus report on the overall progression of the reaction, as reviewed [57]. Sigmoidal curves are typically observed and may be divided into three phases: the lag phase, the transition phase and the final plateau. However, none of these three phases can be ascribed to a single microscopic process. All microscopic processes underlying the overall reaction are active during all phases of the reaction [32, 47, 57]. Typical samples used in aggregation studies contain $6 \cdot 10^8$–$3 \cdot 10^{16}$ monomers (1–500 µl of 1 nM – 100 µM). Therefore, the reaction can be described in terms of rate constants and activities and the reaction time course will be the same each time an identical sample is studied [42, 58].

For a reaction starting from Aβ42 monomer only, the time span where only primary nucleation takes place extends ca 10^{-7} % into the lag phase [57]; after this elongation of fibrils and thereby secondary nucleation takes place. The monomer concentration stays close to constant during the entire lag phase and primary nucleation occurs with close to constant rate during the entire lag phase. The rate of primary nucleation is for the majority of the reaction time course overshadowed by the many orders of magnitude faster secondary nucleation, which occurs with highest rate at the mid-point of the macroscopic transition where both fibril and monomers are present at ca. 50 % of their maximum concentration. Thus if any of the three macroscopic phases should be called the nucleation phase, that would be the transition phase.

The duration of the lag time is in most cases not strongly influenced by the primary nucleation rate, but rather by growth and proliferation by secondary nucleation processes. After establishing that Aβ42 aggregation is dominated by monomer-dependent secondary nucleation [1], it was found that Aβ42 fibrils can be detected from very early stages of the lag phase [59]. The fibril concentration grows almost exponentially during the lag phase (proportional to $\cosh(k \cdot t) - 1$) [32, 59]), but cannot be detected by most bulk techniques until on the order of 1 % of the monomers have been converted to fibrils, i.e. at the end of the lag phase. Fibrils during the lag phase can be observed using cryo-TEM or inferred using trapping in centrifugal filters and seeding of fresh monomer [59].

Factors modulating secondary nucleation

The rate of secondary nucleation depends on the interfacial energy, the molar volume of the solid phase and the difference in chemical potential between the solution and solid phase [60, 61]. The rate and mechanism of secondary nucleation is thus highly sensitive to extrinsic factors such as temperature and solution composition, as well as to intrinsic factors such as point mutations and extensions and truncations of the peptide sequence. A remarkable example is the effect of temperature, in which case it was found that secondary nucleation is relatively insensitive to temperature. While primary nucleation and elongation both proceed at higher rate the higher the temperature; secondary nucleation has a weak opposite temperature dependence with slightly higher rate at lower temperature [62]. Increasing the ionic strength of the solution increases the rate of aggregation by screening the electrostatic repulsion between monomers and between monomers and fibrils [63, 64]. Moreover, screening of electrostatic repulsion speeds up the association of monomers with fibrils more than nucleation and product release, leading to Michaelis Menten-like kinetics, a-kin to enzyme kinetics, and saturation of the rate of secondary nucleation at high monomer concentration [64]. The fibril surface acts as a catalyst; monomer is the substrate with affinity for the catalytic surface, the nucleated species is the product, and product release becomes the rate-limiting step at high monomer concentration. Similar behavior is observed close to neutral pH [52]. The search for intrinsic factors may be inspired both by the occurrence of early-onset familial mutations and the information provided by solid-state NMR structures [30] on which residue side-chains are exposed on the Aβ42 fibril (Fig. 3). Increased rate of secondary nucleation with saturation at high monomer concentration has been observed for familial mutations making the peptide less negatively charged [51] or increasing

the hydrophobicity of the N-terminus [52], and for the C-terminally truncated form, Aβ40 [2]. Extension of the unstructured N-terminus of Aβ42, on the contrary, slows down both primary and secondary nucleation [48]. Importantly, secondary nucleation of Aβ42 is prevalent also in a body fluid such as cerebrospinal fluid [65] (Frankel et al., unpublished) and in the presence of phospholipid membranes [66, 67]. A recent study of truncated α-syn variants shows that removal of the negatively charged C-terminus moves the range for secondary nucleation towards neutral pH [68].

Specificity of secondary nucleation

Secondary nucleation happens on the surface of an aggregate formed from the same kind of monomers and is thereby by definition specific. It is still of interest to ask whether fibrils formed of closely related peptides, such as Aβ length variants, or fibrils formed from a more distant protein, catalyze on their surface the nucleation of one or the other protein. A striking example is provided by Aβ40 and Aβ42, which on their own display significant secondary nucleation. Several studies have found an acceleration of Aβ40 aggregation in the presence of Aβ42 monomers and a slight retardation of Aβ42 aggregation in the presence of Aβ40 monomers ([69] and references therein). When produced in ultra-pure form as recombinant peptides, each monomer type is only accelerated by fibrils of the same length variant and no cross-catalysis is observed [69]. This signifies that Aβ42 is unable to copy the structure of the Aβ40 fibril and Aβ40 is unable to copy the structure of the Aβ42 fibril. An example of more distant proteins is provided by Aβ42 and α-syn. In this case, heterogeneous primary nucleation of Aβ42 aggregates seems to occur on fibrillar α-synuclein [70].

Inhibition of amyloid formation – a mechanistic perspective

Significant efforts are spent trying to find inhibitors of amyloid formation, with anticipation that this could provide therapeutic intervention of amyloid diseases. Recent advances in finding the underlying microscopic steps in amyloid formation now makes it possible to tailor inhibitors to specifically suppress certain steps [3, 71]. This is facilitated by the fact that the effect on the macroscopically observable aggregation curve will be very different depending on which microscopic process is inhibited (Fig. 7a–c). The identification of secondary nucleation as a major generator of toxicity makes it especially valuable to find compounds that interfere with this step as this can limit the total number of toxic species formed (Fig. 7e). Inhibition of primary nucleation may also be beneficial because although such approach may not decrease the number of oligomers formed over time, it can significantly delay their appearance and thereby the toxicity (Fig. 7d). In contrary, inhibition of elongation may increase the number of oligomers formed over time, because a larger fraction of the reactive flux proceeds via secondary nucleation (Fig. 7e).

A key experiment for pinpointing which microscopic process is reduced by a specific inhibitor, involves monitoring aggregation kinetics at a fixed initial monomer concentration of the amyloid protein in the absence and presence of inhibitor at a series of concentrations. The data are then fitted assuming that either one rate constant is reduced while the others remain unchanged to see if any of those scenarios agree with the data. If needed more than one rate constant may be allowed to take curve-specific values. Light and heavy seeding in the absence and presence of inhibitor will then strengthen the conclusions, if relevant.

The Brichos chaperone – the first example of a secondary nucleation inhibitor

The first secondary nucleation inhibitor of Aβ aggregation to be discovered was the Brichos chaperone domain from lung surfactant protein C [3]. The natural function of this domain is to prevent amyloid formation of a

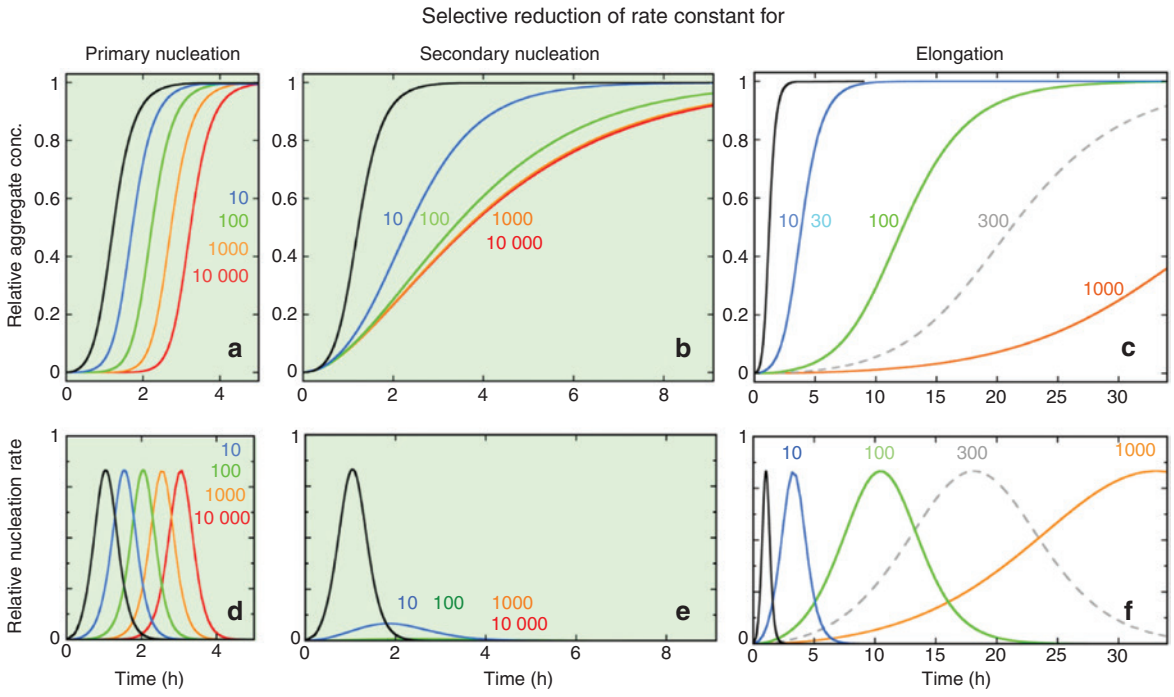

Fig. 7: Predicted changes in the macroscopic aggregation curves (panels a–c) and oligomer generation (sum of primary and secondary nucleation, panels (d–f) upon selective reduction of the rate constants of (a) primary nucleation (k_n), (b) secondary nucleation (k_2) and (c) elongation (k_+) calculated using the Amylofit platform [86]. All calculations assumed that the reaction was initiated at time 0 from a solution containing 3 μM Aβ42 monomer. (d–f) The reference black curve in each panel (a–f) was calculated using the rate constants measured for Aβ42 in 20 mM sodium phosphate buffer with 0.2 mM EDTA, pH 8.0, 37 °C: $k_n = 3.10^{-1}\ M^{-1}\ s^{-1}$, $k_2 = 1 \cdot 10^4\ M^{-1}\ s^{-1}$, $k_+ = 3 \cdot 10^6\ M^{-1}\ s^{-1}$ [1]. Each colored curve was calculated with two rate constants were fixed at the values above, and the rate constant for the process indicated above the panel reduced by a series of factors as indicated next to each curve. The nucleation rate of over time was calculated using the concentration of fibril as displayed in panels a–c, and the concentration of monomer as 3 μM (1 – f), where f is the fraction of monomers in fibrils.

surface active segment of the lung surfactant protein C, but the domains has a profound effect also on the aggregation of Aβ40 and Aβ42 [72]. The first indication that the Brichos domain is a secondary nucleation inhibitor came from the failure to fit aggregation kinetics data for Aβ42 in the presence of Brichos, at a range of concentrations, assuming either that Brichos reduces the rate constant for primary nucleation (Fig. 8a) or that it reduces the rate constant for elongation (Fig. 8b). However, a remarkable agreement between the calculated curves and the observed data was found if the rate constant for secondary nucleation was reduced (Fig. 8c, [3]).

Selective inhibition of secondary nucleation

Indeed, the data at the highest Brichos concentration (red data in Fig. 8) could be fitted if the rate constant for secondary nucleation was set to zero while the rate constants for primary nucleation and elongation were kept at the same values as in the absence of Brichos. This remarkable selectivity, complete inhibition of one microscopic step with no observable effect on other steps, was further challenged by adding higher concentration of Brichos, up to three times the concentration where complete inhibition is observed, but no additional effects were observed [3]. The Brichos chaperone domain from lung surfactant protein C is thus highly selective and suppresses secondary nucleation with no effect on primary nucleation or elongation. Brichos domains are found in many other proteins with amyloidogenic segments, for example in the protein Bri2. At high concentration of Bri2-Brichos, additional effects on elongation were observed [71].

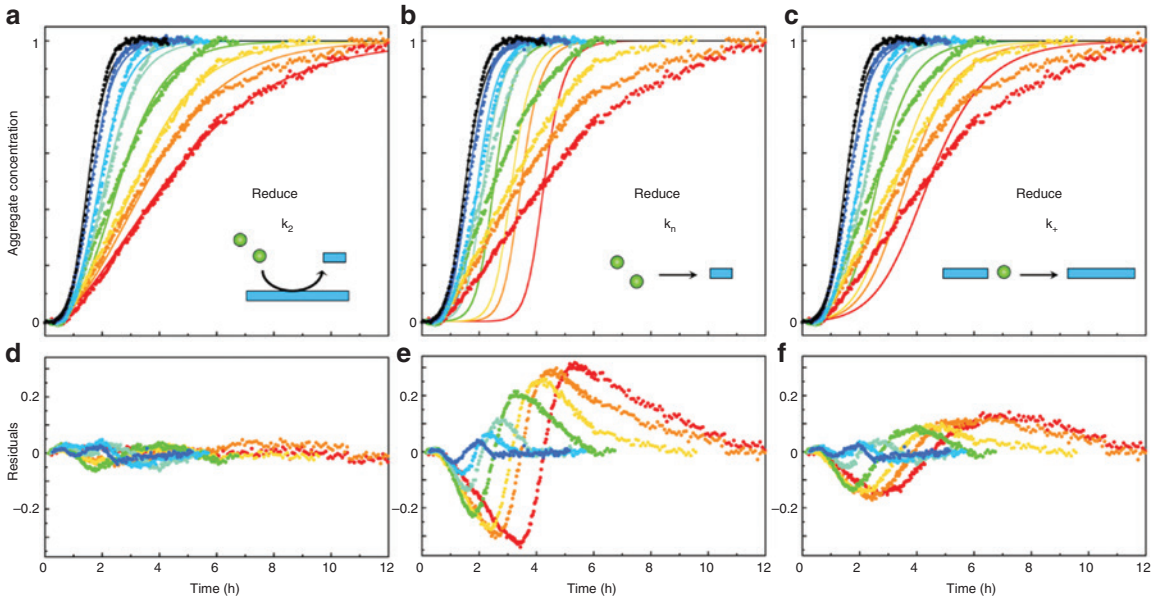

Fig. 8: Aggregation kinetics of 3 μM Aβ42 in the absence (black) or presence of 0.1–2 μM pro-SPC Brichos (colors). The best possible fits for three cases are shown: (a) selective reduction of the rate constant for secondary nucleation, (b) selective reduction of the rate constant for primary nucleation and (c) selective reduction of the rate constant for elongation. The residuals of the fits are shown in panels d–f, under the respective fit. Data from Ref. [3].

Seeded experiments confirm inhibition of secondary nucleation

The effect on secondary nucleation was validated by experiments in which the addition of small amounts of preformed fibrils (seeds) were added to bypass the primary nucleation process, resulting in almost all new fibrils being generated through secondary nucleation. These experiments were repeated in the absence and presence of Brichos (Fig. 9). The remarkable shortening of the lag phase already at low seed concentration as observed in the absence of Brichos (Fig. 9a), was completely abolished in the presence of Brichos (Fig. 9b), thus the data confirmed that the presence of Brichos inhibited the fibril-dependent nucleation process [3].

Binding experiments indicate interaction of Brichos with fibrils

Secondary nucleation inhibitors could in principle act by biding to fibrils, thereby competing with Aβ monomers for binding to the catalytic sites, or by interacting with newly formed aggregates preventing their

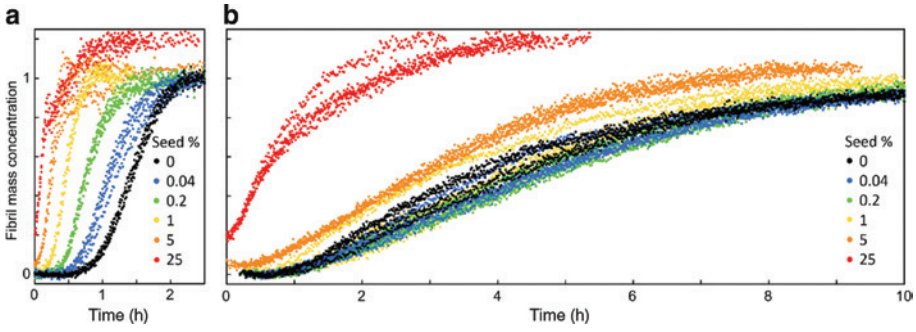

Fig. 9: Seeded aggregation kinetics of 3 μM Aβ42 in the absence (a) or presence of 2 μM pro-SPC Brichos (b). Four replicates of each solution are shown, and the seed concentrations (in monomer units in % of the free monomers) are 0 (black), 0.04 % (blue), 0.2 % (green), 1 % (yellow), 5 % (orange) and 25 % (red). Data from Ref. [3].

conversion and growth. The results of surface plasmon resonance studies imply that Brichos binds with relatively high affinity to immobilized fibrils (K_D was estimated to be 40 nM) but not to immobilized monomers (Fig. 10a, [3]). Using immunogold-labeled anti-Brichos antibody, the binding to fibrils was also inferred from transmission electron microscopy images (Fig. 10b, [3]).

Brichos reduces toxicity during Aβ42 aggregation

A critical feature of secondary nucleation is that it can generate significant concentrations of oligomeric aggregates (Fig. 7d–f), and oligomers are found to be toxic to neuronal cells [73, 74]. Several studies have shown that secondary nucleation generates toxicity, through a reaction involving both fibril seeds and monomer, see for example [1, 3, 75]. The toxicity emerging during aggregation of Aβ42 was found to be drastically reduced in the presence of Brichos (Fig. 11). The efficacy of Brichos to limit toxicity was observed in

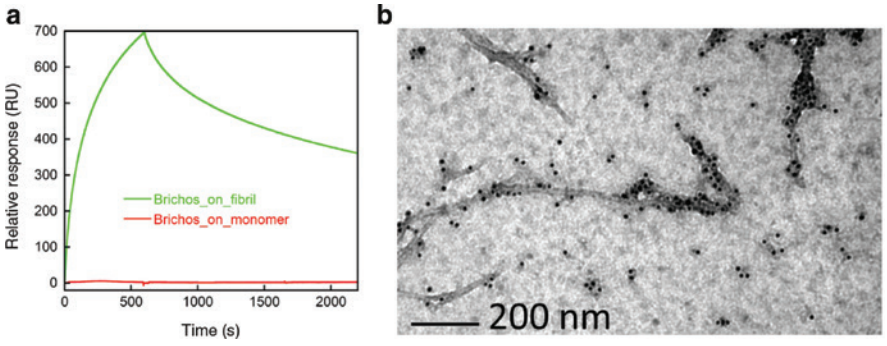

Fig. 10: Brichos binding to fibrils. Surface plasmon resonance studies (a) with Brichos injected for 700 s followed by buffer flow, indicate that Brichos binds with high affinity to immobilized Aβ42 fibrils (green trace) but not to immobilized Aβ42 monomers (red trace). 1 RU = 1 pg/mm^2. (b) transmission electron microscopy image of fibrils formed in the presence of Brichos and incubated with gold-labeled anti-Brichos antibody. Data from Ref. [3].

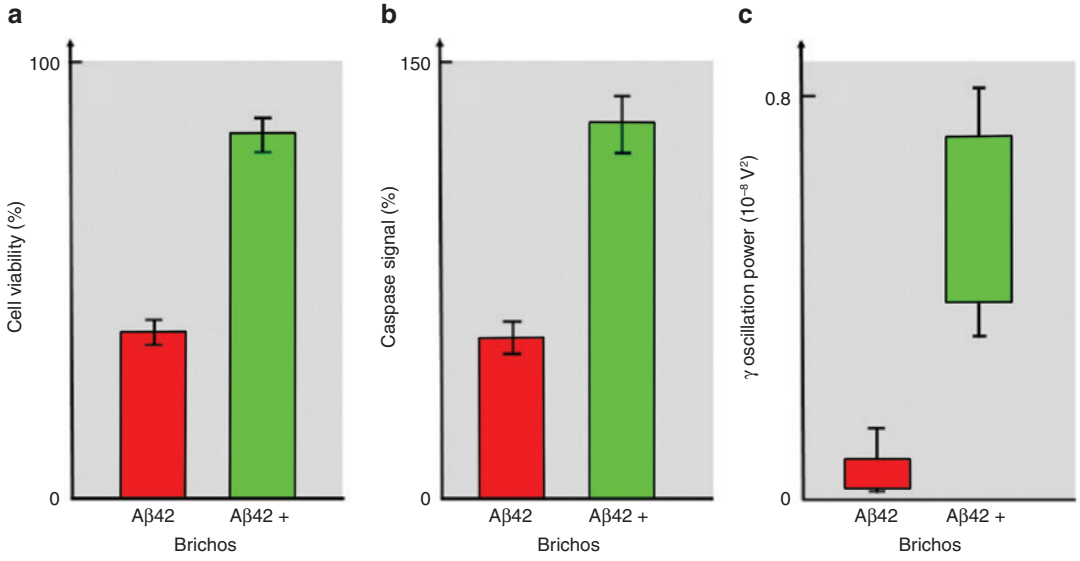

Fig. 11: Toxicity of Aβ42 in the absence (red) and presence (green) of pro-SPC Brichos as measured using assays for MTT reduction (a) and caspase activity (b) in cell lines, and electrophysiology measurements of gamma oscillations in brain slices (c). Panels A and B show averages and standard deviations over four replicates, and panel C shows box and whisker plots over 8 replicates. Data from Ref. [3].

experiments using cell lines [3], mouse brain slices [3] and fruit flies [76]. The experiments with cell lies and mouse brain slices were setup to study the toxicity emerging during seed-catalyzed aggregation reactions. The toxicity to cells was evaluated using MTT and caspase assays, which are complicated by the fact that the entire life and metabolism of the cells is translated to a single spectroscopic readout. Electrophysiology measurements of γ oscillations in mouse brain slices may provide a more direct readout of the effect on cellular processes connected to memory and learning. Yet, the effects arising during an ongoing Aβ42 aggregation process were diminished in the presence of Brichos in both systems (Fig. 11, [3]). Transgenic flies (*Drosophila melanogaster*) expressing human Aβ42 and Brichos in the central nervous system displayed improved lifespan and locomotor function compared to flies expressing only Aβ42 [76]. Brichos was found to bind to Aβ42 deposits in the brain thereby reducing the toxic effect although significant Aβ42 aggregation was taking place in both kinds of transgenic files.

Phage display libraries in search of secondary nucleation inhibitors

Inspired by the successful identification of Brichos as a selective secondary nucleation inhibitor, which very effectively limits toxicity, we set out to explore whether additional proteins with the same effect could be identified. To this end we used phage display libraries of antibody fragments, so called single chain variable domains, scFvs [77, 78]. Three rounds of phage display selection were set up with intervening amplification in *Escherichia coli* (Fig. 12, [79]). In each round, we first used immobilized Aβ42 monomers to remove monomer-binding scFvs (Fig. 12b) and then used immobilized Aβ42 fibrils to capture fibril-binders among the remaining scFvs (Fig. 12d). Surface plasmon resonance using sensor surfaces with immobilized fibrils provided a first ranking of a large number of scFv-phages from culture supernatants, and later of a smaller collection of scFvs free from phages from the most promising clones. These were then used in aggregation kinetics analyses to find candidate scFvs that selectively inhibit secondary nucleation (Fig. 13). Among seven tested candidates, four had the desired property of selective inhibition of secondary nucleation [79]. Two additional

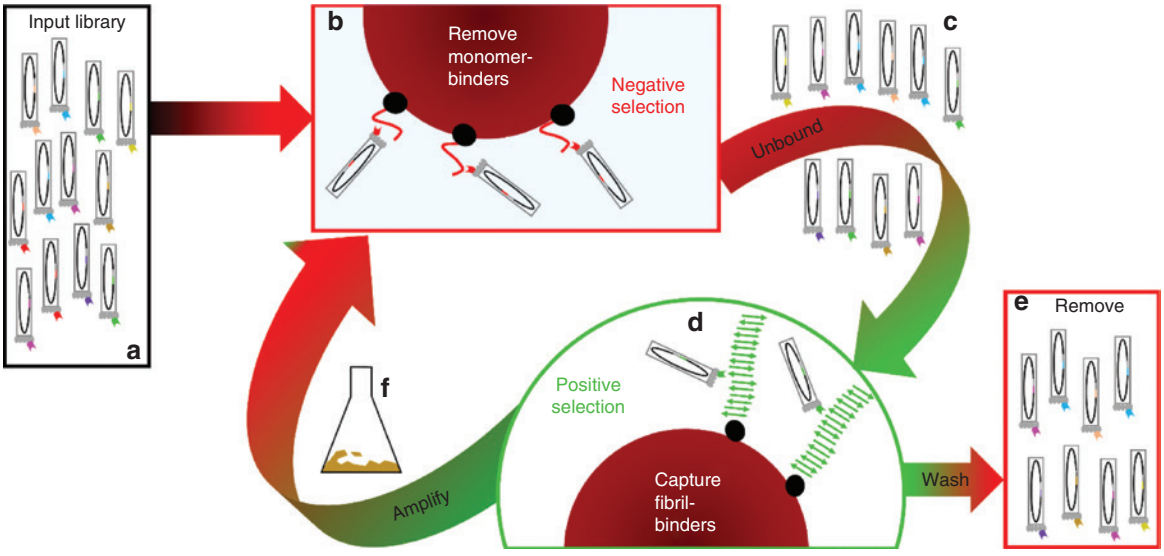

Fig. 12: Phage display selection of fibril-specific single-chain antibody fragments (scFVs). An input library of phages expressing scFvs on their surface in fusion with protein III (a) is added to magnetic beads coated with Aβ42 monomer (b). Monomer-binders are thereby removed and the unbound phages (c) are added to magnetic beads coated with Aβ42 fibrils (d). Unbound phages are removed by extensive washing (e), and bound phages are eluted with acid, neutralized and used to infect *Escherichia coli* for amplification of an enriched library (f). The enriched library is used as an input in a second round. The whole procedure is repeated for three rounds [79].

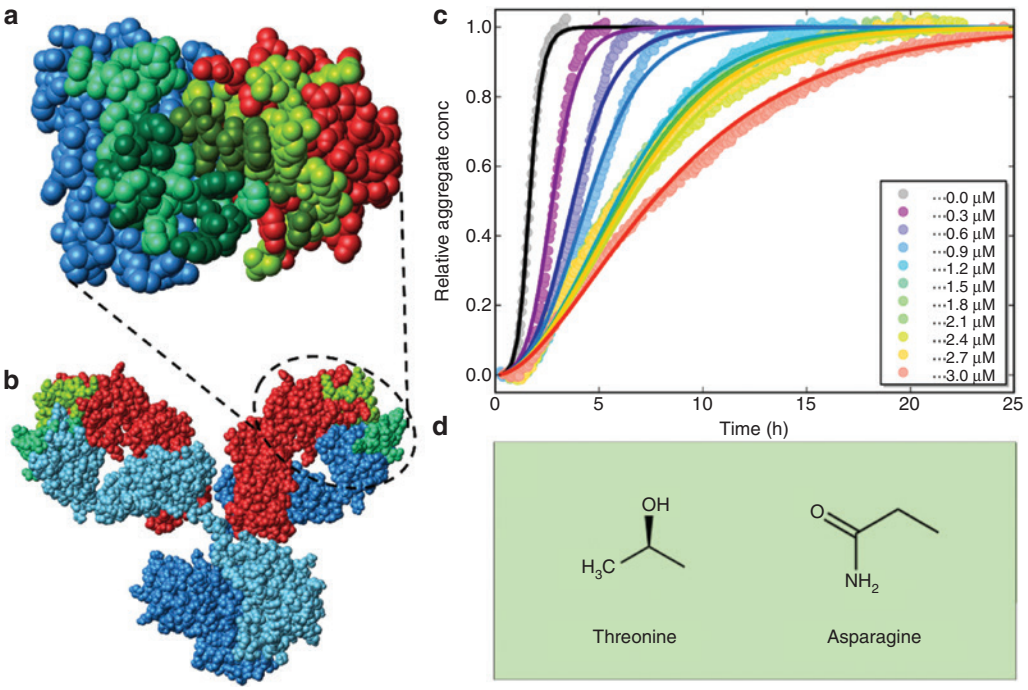

Fig. 13: Fibril specific svFvs inhibit secondary nucleation. Space-filling model of an scFv (a) and an intact IgG (b) with the heavy chain in blue, light chain in red and the variable loops in green. In panel A, the residues which where varied in the input library are shown in darker green. (c) Aggregation kinetics of 3 µM Ab42 in the absence (black) and presence (colors) of increasing concentration of one of the fibril specific scFvs (called clone I48 [79]). (d) Two different input libraries were used (Thomlinson I and J) and in both cases, threonine and asparagine were found to be upregulated in the variable positions of the scFvs that specically inhibit secondary nucleation [77]. The Figure was prepared using Molmol [85].

ones inhibited secondary nucleation at low scFV concentration but secondary nucleation and elongation at high scFV concentration, and were therefore discarded. Besides illustrating the power of kinetics to be able to remove scFvs that might potentially increase rather than decrease toxicity, the dual behavior of these two scFvs in different concentration regimes also provide key information that the sites for secondary nucleation and elongation must be different [79].

Designed antibodies and small molecules as secondary nucleation inhibitors

Secondary nucleation inhibitors can also be produced through rational design of antibody fragments towards discrete regions of the Aβ42 sequence [80]. S100B was recently reported to inhibit secondary nucleation of Aβ42 in the presence of calcium ions [81]. In addition, a number of small molecules have been identified that display inhibition of secondary nucleation of Aβ42 or Aβ40 [82–84].

Consequences of secondary nucleation – intra-cellular targets of toxic oligomers

A major consequence of secondary nucleation is the generation of oligomeric aggregates that may in turn be taken up in cells [73, 74] and interact with various biomolecules. We therefore decided to test if diffusible aggregates present in Aβ42 solutions would interact with any specific proteins using protein

arrays on microscope slides with close to 10,000 different proteins immobilized in duplicate. To avoid false positives due to sedimenting fibrils, we placed the array on top of the solution with an ongoing aggregation reaction (Fig. 14, [85]). The rate constants determined for Aβ42 in physiological salt solution were used to guide the experimental setup to cover the time-frame during which the majority of toxic oligomers are generated, which turns out to be the transition phase of the macroscopically observable aggregation curves (Fig. 14a). This approach lead to the identification of one target significantly above the noise – glycogen synthase kinase 3α (GSK3α, [85], Fig. 14b,c), and the interaction of GSK3α with Aβ42 oligomers was validated using thermophoresis, surface plasmon resonance and phosphorylation assays. The results are intriguing because this kinase may phosphorylate protein tau, which is another main player in Alzheimer's disease.

Kinetic analysis

The experimental work reviewed here has been executed in close collaboration with scientists developing kinetic models and analysis procedures [44–47, 86]. This work used as a starting point the coupled differential equations describing possible composite steps that include as reactants monomers and/or all possible sizes of oligomers and fibrils:

i) primary nucleation of monomer only, with rate constant k_n and reaction order n_c in monomer
ii) secondary nucleation of monomers on the surface of fibrils, with rate constant k_2 and reaction order n_2 in monomer
iii) elongation by monomer addition at fibril ends, with rate constant k_+
iv) fibril breakage leading to exposure of new ends for elongation, with rate constant k_-.

Due to the complexity of the models, data analysis was performed in a global manner, such that the equations fit the kinetics at several monomer and seed concentrations simultaneously. An interface for these analyses is now available online [86].

Fibril morphology in relation to secondary nucleation

Polymorphism among amyloid-fibrils of the same peptide is a well-known phenomenon. Individual fibrils may differ in terms of the local packing of monomers, which propagates to distinct structural features at

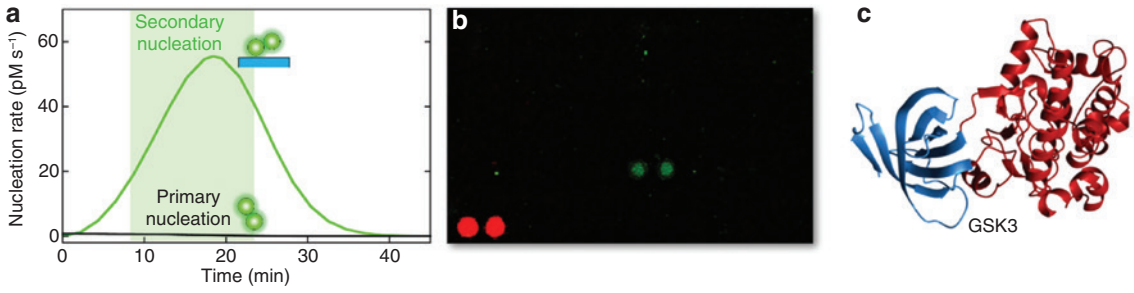

Fig. 14: Identification of GSK3α as an intracellular target of Aβ oligomers [85]. (a) Using the rate constants, determined in physiological salt buffer at 37 °C it was calculated that most of the toxic oligomers would be generated between 8 and 23 min of a reaction starting from 5 μM monomer at time zero. (b) A protein array microscope slide was placed during this time window on top of a solution with an ongoing aggregation reaction of 5 μM Aβ42 in physiological salt buffer at 37 °C, with a minor fraction being fluorophore labeled to facilitate imaging leading to identification of one putative target, GSK3α, significantly above background (c).

longer length scales such as twist distance and the number of filaments per fibril [87]. The formation of a specific polymorph is governed by its nucleation and growth rates in comparison with other polymorphs. Several polymorphs may co-exist in the same solution; however, the most stable form will eventually dominate the solution since the less stable polymorphs dissolve more quickly than the more stable ones [88]. Industrial crystallization protocols utilize secondary nucleation as a key process to achieve a product with one dominating polymorph [89]. It is also likely that prion propagation, i.e. copying of a parent fibril structure by new aggregates forming in the presence of the parent, may originate from monomer-dependent secondary nucleation [33]. In general, high purity of amyloid protein samples counteracts polymorphism and governs the formation of the same fibril structure in independent replicates of the solution. This is illustrated in the case of Aβ42 fibrils, where two groups separately produced and purified Aβ42 monomers, which were found to self assemble into the same fibril structure [36, 90, 91]. One group used parallel non-seeded samples [36, 90] and the other group used several rounds of seeding [91], indicating that the fibril form with fastest secondary nucleation, i.e. the one that wins over time during repeated seeding, is also the one that forms spontaneously in pure samples.

A brief not on solubility, stability, metastability, saturation, supersaturation, phase transitions and phase separation

Self-assembly into amyloid fibrils involves the spontaneous association of monomers. The monomer concentration, temperature and solution conditions govern whether a solutions is stable, metastable or unstable [16, 17, 92]. At concentrations below the solubility limit, S_0, sometimes called saturation concentration, the solution remains monomeric for infinite time and this is the thermodynamically most stable state for a homogeneous solution of monomers. In a typical aggregation kinetics experiment, a supersaturated solution, i.e. a solution of monomers at a concentration above S_0, is created by a sudden change in temperature or pH, or by dilution into aqueous solution from an organic solvent. Under supersaturated conditions, the most stable state is a two-phase system, in which an aggregate phase co-exists with a solution phase of monomers. The system may remain metastable for some time; for large enough system, as in the experiments discussed in this review, this time is highly predictable and reproducible. For the same reason, the width of the metastable zone is time-dependent in a highly reproducible manner for macroscopic samples [92]. Deviation from reproducible kinetics implies that impurities or other perturbations differ from sample to sample. The aggregation of Aβ42 displays the characteristics of a phase transition; at the end of the reaction there is a relatively constant concentration of monomer (ca. 20 nM) co-existing with fibrillar aggregates over a wide range of total monomer concentrations [42]. Huntingtin aggregation has been described as a co-existence of three phases with monomers and oligomers in one liquid phase, large spheres of ca 25 nm diameter in another liquid phase, and fibrils in a solid phase [93]. The presence of ligands, polymers or other substances that preferentially bind or adsorb to the species in one phase are special cases of altered solution conditions that can alter the solubility and shift phase boundaries [92, 94, 95]. It is thus relevant to evaluate whether inhibitors of secondary nucleation shift the equilibrium distribution between free monomers and fibrils. There is also increasing evidence of liquid-liquid phase separations in biology [96], which may be linked to nucleation of fibril formation [97, 98].

A note on the use of ThT

The main drawback of using ThT to monitor amyloid formation is the indirect nature of the signal. Direct methods such as NMR spectroscopy to monitor monomer concentration, or direct fluorescence [99] or fluorescence polarization [56] to monitor fibril formation, have the advantage of being non-perturbing, but may suffer from lower signal to noise. For Aβ42 with high aggregation propensity, requiring studies in a low

peptide concentration regime, ThT is selected as a practical compromise to report on the overall progression of the reaction. To allow for the use of ThT, we optimized its concentration to an interval (5–20 μM) where its fluorescence signal is linearly dependent on the mass concentration of fibrils [1]. Moreover, by comparing time courses for samples to which ThT had been at different time-points after initiating the reaction, and finding near identity, it was concluded that the presence of ThT in this concentration range does not affect the fibril formation kinetics [40]. The latter is surprising, as any substance that binds to one phase in a transition will affect its equilibrium. Probably ThT binds to fibrils after they form and thereby does not affect the formation kinetics, and if the very slow back-reaction (dissociation of fibrils) is made even slower it does not affect the kinetics of fibril formation, which occurs on shorter time scales.

Acknowledgments: The results presented here relies on work by a large number of scientists including from Lund University: Erik Hellstrand, Risto Cukalevski, Xiaoting Yang, Olga Szczepankiewicz, Tanja Weiffert, Kalyani Sanagavarapu, Mattias Törnquist, Tinna Palmadottir, Christopher Dunning, Katja Bernfur, Anders Malmendal, Cecilia Emanuelsson, Veronica Lattanzi, Rebecca Frankel, Martin Lundquist, Tommy Cedervall, Thom Leiding, Eva Thulin, Hanna Nilsson, Birgitta Frohm, from Cambridge University: Tuomas Knowles, Sam Cohen, Georg Meisl, Paolo Arosio (now at ETH Zürich), Thomas Michaels, Francesco Aprile, Pietro Sormanni, Michele Vendruscolo, Christopher Dobson, and from Karolinska Institute, Stockholm: Jenny Presto, Jan Johansson, André Fishan, Lisa Dolfe, Henrik Biverstål, from MIT: Robert Griffin, Michael Colvin, Robert Silvers, and from University College Dublin: Dominic Walsh (now at Harvard), David O'Connell and Gavin McGauran. The work was funded by an ERC Advanced Grant, the Swedish Research Council, Alzhemierfonden and NanoLund. Scientific discussions with Lennart Lindfors, Astra Zeneca, Mölndal, are gratefully acknowledged.

Article note: A special collection of invited papers by recipients of the IUPAC Distinguished Women in Chemistry and Chemical Engineering Awards.

References

[1] S. I. Cohen, S. Linse, L. M. Luheshi, E. Hellstrand, D. A. White, L. Rajah, D. E. Otzen, M. Vendruscolo, C. M. Dobson, T. P. Knowles. *Proc. Natl. Acad. Sci. USA* **110**, 9758 (2013).
[2] G. Meisl, X. Yang, E. Hellstrand, B. Frohm, J. B. Kirkegaard, S. I. Cohen, C. M. Dobson, S. Linse, T. P. Knowles. *Proc. Natl. Acad. Sci. USA* **111**, 9384 (2014).
[3] S. I. Cohen, P. Arosio, J. Presto, F. R. Kurudenkandy, H. Biverstål, L. Dolfe, C. Dunning, X. Yang, B. Frohm, M. Vendruscolo, J. Johansson, C. M. Dobson, A. Fisahn, T. P. Knowles, S. Linse. *Nat. Struct. Mol. Biol.* **22**, 207 (2015).
[4] M. Törnquist, T. C. T. Michaels, K. Sanagavarapu, X. Yang, G. Meisl, S. I. A. Cohen, T. P. J. Knowles, S. Linse. *Chem. Commun. (Camb).* **54**, 8667 (2018).
[5] C. Galvagnion, A. K. Buell, G. Meisl, T. C. Michaels, M. Vendruscolo, T. P. Knowles, C. M. Dobson. *Nat. Chem. Biol.* **11**, 229 (2015).
[6] S. Linse, C. Cabaleiro-Lago, W. F. Xue, I. Lynch, S. Lindman, E. Thulin, S. E. Radford, K. A. Dawson. *Proc. Natl. Acad. Sci. USA* **104**, 8691 (2007).
[7] R. Vácha, S. Linse, M. Lund. *J. Am. Chem. Soc.* **136**, 11776 (2014).
[8] S. Campioni, G. Carret, S. Jordens, L. Nicoud, R. Mezzenga, R. Riek. *J. Am. Chem. Soc*. **136**, 2866 (2014).
[9] P. Scheltens, K. Blennow, M. M. Breteler, B. De Strooper, G. B. Frisoni, S. Salloway, W. M. Van der Flier. *Lancet* **388**, 505 (2016).
[10] F. Chiti, C. M. Dobson. *Annu. Rev. Biochem*. **75**, 333 (2006).
[11] D. Eisenberg, M. Jucker. *Cell* **148**, 1188 (2012).
[12] T. P. Knowles, M. Vendruscolo, C. M. Dobson. *Nat. Rev. Mol. Cell. Biol.* **15**, 384 (2014).
[13] F. Chiti, C. M. Dobson. *Annu. Rev. Biochem*. **86**, 27 (2017).
[14] P. C. Ke, M. A. Sani, F. Ding, A. Kakinen, I. Javed, F. Separovic, T. P. Davis, R. Mezzenga. *Chem. Soc. Rev.* **46**, 6492 (2017).
[15] G. D. Botsaris. *Industrial Crystallization*, pp. 3–22, Springer, Boston (1976).
[16] H. A. Miers, P. Isaac. *Chem. Soc. J.* **89**, 413 (1906).
[17] A. McPherson. *Crystallization of Biological Macromolecules*. CSHL Press, Cold Spring Harbor (1999).
[18] S. G. Agrawal, A. H. J. Paterson. *Chem. Eng. Commun.* **202**, 98 (2015).
[19] D. K. Kondepudi, R. J. Kaufman, N. Singh. *Science* **250**, 975 (1990).

[20] R. Y. Waghmare, J. N. Webb, T. W. Randolph, M. A. Larson, C. E. Glatz. *J. Cryst. Growth* **208**, 678 (2000).
[21] A. Srisa-nga, A. E. Flood, E. T. White. *Cryst. Growth Des.* **6**, 795 (2006).
[22] S. Tait, E. T. White, J. D. Litster. *Cryst. Growth Des.* **9**, 2198 (2009).
[23] R. Chow, R. Blindt, R. Chivers, M. Povey. *Ultrasonics* **43**, 227 (2005).
[24] J. Anwar, S. Khan, L. Lindfors. *Angew. Chem. Int. Ed. Engl.* **54**, 14681 (2015).
[25] G. L. Gardner, G. K. Nancollas. *J. Dent. Res.* **55**, 342 (1976).
[26] R. Zong, Y. Wang, S. Shi, Y. Zhu. *PCCP* **16**, 4236 (2014).
[27] P. Cubillas, M. W. Anderson. in *Zeolites and Catalysis, Synthesis, Reactions and Applications*, A. Corma, S. Zones (Eds.), pp. 1–56, WILEY-VCH Verlag GmbH & Co. KGaA, Weinheim, **1**, (2010).
[28] J. Garside, R. J. Davey. *Chem. Eng. Comm.* **4**, 393 (1980).
[29] E. Verdurand, C. Bebon, D. Colson, J.-P. Klein, A.-F. Blandin, J.-M. Bossoutrot. *J. Cryst. Growth* **275**, e1363 (2005).
[30] F. A. Ferrone, J. Hofrichter, H. R. Sunshine, W. A. Eaton. *Biophys. J.* **32**, 361 (1980).
[31] M. F. Bishop, F. A. Ferrone. *Biophys. J.* **46**, 631 (1984).
[32] F. A. Ferrone, J. Hofrichter, W. A. Eaton. *J. Mol. Biol.* **183**, 611 (1985).
[33] L.E. Orgel. *Chem. Biol.* **3**, 413 (1996).
[34] The IUPAC Gold book. http://goldbook.iupac.org/html/M/M03804.html, Accessed 17 January 2019.
[35] When models are tested that include different number of parameters, the obained improvement of the error square sum may be validated using an f-test, taking into acocunt the degrees of freedom in the fit (i.e. the number of parameters relative to the number o data points): P. R. Bevington, D. K. Robinsson Data Reduction and error analysis for the physicla sciences. WCB/McGraw-Hill (1992).
[36] M. T. Colvin, R. Silvers, Q. Z. Ni, T. V. Can, I. Sergeyev, M. Rosay, K. J. Donovan, B. Michael, J. Wall, S. Linse, R. G. Griffin. *J. Am. Chem. Soc.* **138**, 9663 (2016).
[37] M. G. Zagorski, J. Yang, H. Shao, K. Ma, H. Zeng, A. Hong. *Methods Enzymol.* **309**, 189 (1999).
[38] V. H. Finder, I. Vodopivec, R. M. Nitsch, R. Glockshuber. *J. Mol. Biol.* **396**, 9 (2010).
[39] D. Walsh, E. Thulin, A. M. Minogue, N. Gustavsson, E. Pang, D. B. Teplow, S. Linse. *FEBS J.* **276**, 1266 (2009).
[40] R. Cukalevski, B. Boland, B. Frohm, E. Thulin, D. Walsh, S. Linse. *ACS Chem. Neurosci.* **3**, 1008 (2012).
[41] L. Shen, T. Adachi, D. Vanden Bout, X. Y. Zhu. *J. Am. Chem. Soc.* **134**, 14172 (2012).
[42] E. Hellstrand, R. Boland, D. M. Walsh, S. Linse. *ACS Chem. Neurosci.* **1**, 13 (2010).
[43] T. P. Knowles, C. A. Waudby, G. L. Devlin, S. I. Cohen, A. Aguzzi, M. Vendruscolo, E. M. Terentjev, M. E. Welland, C. M. Dobson. *Science* **326**, 1533 (2009).
[44] S. I. Cohen, M. Vendruscolo, M. E. Welland, C. M. Dobson, E. M. Terentjev, T. P. Knowles. *J. Chem. Phys.* **135**, 065105 (2011).
[45] S. I. Cohen, M. Vendruscolo, C. M. Dobson, T. P. Knowles. *J. Chem. Phys.* **135**, 065106 (2011).
[46] S. I. Cohen, M. Vendruscolo, C. M. Dobson, T. P. Knowles. *J. Chem. Phys.* **135**, 065107 (2011).
[47] S. I. Cohen, M. Vendruscolo, C. M. Dobson, T. P. Knowles. *J. Mol. Biol.* **421**, 160 (2012).
[48] O. Szczepankiewicz, B. Linse, G. Meisl, E. Thulin, B. Frohm, C. Sala Frigerio, M. T. Colvin, A. C. Jacavone, R. G. Griffin, T. P. Knowles, D. M. Walsh, S. Linse. *J. Am. Chem. Soc.* **137**, 14673 (2015).
[49] C. Dammers, M. Schwarten, A. K. Buell, D. Willbold. *Chem Sci.* **8**, 4996 (2017).
[50] B. Bolognesi, S. I. Cohen, P. Aran Terol, E. K. Esbjörner, S. Giorgetti, M. F. Mossuto, A. Natalello, A. C. Brorsson, T. P. Knowles, C. M. Dobson, L. M. Luheshi. *ACS Chem. Biol.* **9**, 378 (2014).
[51] G. Meisl, X. Yang, B. Frohm, T. P. Knowles, S. Linse. *Sci. Rep.* **6**, 18728 (2016).
[52] X. Yang, G. Meisl, B. Frohm, E. Thulin, T. P. J. Knowles, S. Linse. *Proc. Natl. Acad. Sci. USA* **115**, E5849 (2018).
[53] A. K. Buell, C. Galvagnion, R. Gaspar, E. Sparr, M. Vendruscolo, T. P. Knowles, S. Linse, C. M. Dobson. *Proc. Natl. Acad. Sci. USA* **111**, 7671 (2014).
[54] R. Gaspar, G. Meisl. A. K. Buell, L. Young, C. F. Kaminski, T. P. J. Knowles, E. Sparr, S. Linse. *Q. Rev. Biophys.* **50**, e6 (2017).
[55] V. Foderà, F. Librizzi, M. Groenning, M. van de Weert, M. Leone. *J. Phys. Chem. B* **112**, 3853 (2008).
[56] S. B. Padrick, A. D. Miranker. *Biocheimistry* **41**, 4694 (2002).
[57] P. Arosio, T. P. Knowles, S. Linse. *Phys. Chem. Chem. Phys.* **17**, 7606 (2015).
[58] B. Linse, S. Linse. *Mol. Biosyst.* **7**, 2296 (2011).
[59] P. Arosio, R. Cukalevski, B. Frohm, T. P. Knowles, S. Linse. *J. Am. Chem. Soc.* **136**, 219 (2014).
[60] Y.-R. Qian, D. Botsaris. *Chem. Eng. Sci.* **52**, 3429 (1997).
[61] D. P. Kondepudi, K. Asakura. *Acc. Chem. Res.* **34**, 946 (2001).
[62] S. I. A. Cohen, R. Cukalevski, R., T. C. T. Michaels, T. C. T., A. Saric, A., M. Törnquist, M. Vendruscolo, C. M. Dobson, A. K. Buell, T. P. J. Knowles, S. Linse. *Nat. Chem.* **10**, 523 (2018).
[63] A. Abelein, J. Jarvet, A. Barth, A. Gräslund, J. Danielsson. *J. Am. Chem. Soc.* **138**, 6893 (2016).
[64] G. Meisl, X. Yang, C. M. Dobson, S. Linse, T. P. J. Knowles. *Chem. Sci.* **8**, 4352 (2017).
[65] R. Koradi, M. Billeter, K. Wuthrich. *J. Mol. Graph.* **14**, 29 (1996).
[66] D.J. Lindberg, E. Wesén, J. Björkeroth, S. Rocha, E. K. Esbjörner. *Bicohim. Biophys. Acta* **1859**, 1921 (2017).
[67] J. Habchi, S. Chia, C. Galvagnion, T. C. T. Michales, M. M. J. Bellaiche, F. S. Ruggeri, M. Sanguanini, I. Idini, J. R. Kumita, E. Sparr, S. Linse, C. M. Dobson, T. P. J. Knowles, M. Vendruscolo. *Nat. Chem.* **10**, 673 (2018).

[68] I. M. van der Wateren, T. P. J. Knowles, A. K. Buell, C. M. Dobson, C. Galvagnion. *Chem. Sci.* **9**, 5506 (2018).
[69] R. Cukalevski, X. Yang, G. Meisl, U. Weininger, K. Bernfur, B. Frohm, T. P. J. Knowles, S. Linse. *Chem. Sci.* **6**, 4215 (2015).
[70] S. Chia, P. Flagmeier, J. Habchi, V. Lattanzi, S. Linse, C. M. Dobson, T. P. J. Knowles, M. Vendruscolo. *Proc. Natl. Acad. Sci. USA* **114**, 8005 (2017).
[71] P. Arosio, T. C. Michaels, S. Linse, C. Månsson, C. Emanuelsson, J. Presto, J. Johansson, M. Vendruscolo, C. M. Dobson, T. P. J. Knowles. *Nat. Commun.* **7**, 10948 (2016).
[72] H. Willander, J. Presto, G. Askarieh, H. Biverstål, B. Frohm, S. D. Knight, J. Johansson, S. Linse. *J. Biol. Chem.* **287**, 31608 (2012).
[73] D. M. Walsh, I. Klyubin, J. V. Fadeeva, W. K. Culle, R. Anwyl, M. S. Wolfe, M. J. Rowan, D. J. Selkoe. *Nature* **416**, 535 (2002).
[74] M. Bucciantini, E. Giannoni, F. Chiti, F. Baroni, L. Formigli, J. Zurdo, N. Taddei, G. Ramponi, C. M. Dobson, M. Stefani. *Nature* **416**, 507 (2002).
[75] A. Jan A, O. Adolfsson, I. Allaman, A. L. Buccarello, P. J. Magistretti, A. Pfeifer, A. Muhs, H. A. Lashuel. *J. Biol. Chem.* **286**, 8585 (2011).
[76] E. Hermansson, S. Schultz, D. Crowther, S. Linse, B. Winblad, G. Westermark. J. Johansson, J. Presto. *Dis. Model Mech.* **7**, 659 (2014).
[77] J. S. Huston, D. Levinson, M. Mudgett-Hunter, M. S. Tai, J. Novotn, M. N. Margolies, R. J. Ridge, R. E. Bruccoleri, E. Haber, R. Crea. *Proc. Natl. Acad. Sci. USA* **85**, 5879 (1988).
[78] T. Clackson, H. R. Hoogenboom, T. P. Bonnert, J. McCafferty, A. D. Griffiths, G. Winter. *Nature* **352**, 624 (1991).
[79] A. Munke, J. Persson, T. Weiffert, E. De Genst, G. Meisl, P. Arosio, A. Carnerup, C. M. Dobson, M. Vendruscolo, T. P. J. Knowles, S. Linse. *Proc. Natl. Acad. Sci. USA* **114**, 6444 (2017).
[80] F. A. Aprile, P. Sormanni, M. Perni, P. Arosio, S. Linse, T. P. J. Knowles, C. M. Dobson, M. Vendruscolo. *Sci. Adv.* **3**, e1700488 (2017).
[81] J. S. Cristóvão, V. K. Morris, I. Cardoso, S. S. Leal, J. Martínez, H. M. Botelho, C. Göbl, R. David, K. Kierdorf, M. Alemi, T. Madl, G. Fritz, B. Reif, C. M. Gomes. *Sci. Adv.* **4**, eaaq1702 (2018).
[82] J. Habchi, S. Chia, R. Limbocker, B. Mannini, M. Ahn, M. Perni, O. Hansson, P. Arosio, J. R. Kumita, P. K. Challa, S. I. Cohen, S. Linse, C. M. Dobson, T. P. Knowles, M. Vendruscolo. *Proc. Natl. Acad. Sci. USA* **114**, E200 (2017).
[83] H. Liu, L. Yu, X. Dong, Y. Sun. *J. Coll. Interface Sci.* **491**, 305 (2017).
[84] S. Chia, J. Habchi, T. C. T. Michaels, S. I. A. Cohen, S. Linse, C. M. Dobson, T. P. J. Knowles, M. Vendruscolo. *Proc. Natl. Acad. Sci. USA* **115**, 10245 (2018).
[85] C. J. Dunning, G. McGauran, K. Willén, G. K. Gouras, D. J. O'Connell, S. Linse. *ACS Chem. Neurosci.* **17**, 161 (2016).
[86] G. Meisl, J. B. Kirkegaard, P. Arosio, T. C. Michaels, M. Vendruscolo, C. M. Dobson, S. Linse, T. P. Knowles. *Nat. Protoc.* **11**, 252 (2016).
[87] A. W. Fitzpatrick, G. T. Debelouchina, M. J. Bayro, D. K. Clare, M. A. Caporini, V. S. Bajaj, C. P. Jaroniec, L. Wang, V. Ladizhansky, S. A. Müller, C. E. MacPhee, C. A. Waudby, H. R. Mott, A. De Simone, T. P. Knowles, H. R. Saibil, M. Vendruscolo, E. V. Orlova, R. G. Griffin, C. M. Dobson. *Proc. Natl. Acad. Sci. USA* **110**, 5468 (2013).
[88] W. Ostwald. *Z. Phys. Chem.* **22**, 289 (1897).
[89] M. O. Besenhard, P. Neugebauer, O. Scheibelhofer, J. G. Khinast. *Cryst. Growth Des.* **17**, 6432 (2017).
[90] M. T. Colvin, R. Silvers, B. Frohm, Y. Su, S. Linse, R. G. Griffin. *J. Am. Chem. Soc.* **137**, 7509 (2015).
[91] M. A. Wälti, F. Ravotti, H. Arai, C. G. Glabe, J. S. Wall, A. Böckmann, P. Güntert, B. H. Meier, R. Riek. *Proc. Natl. Acad. Sci. USA* **113**, E4976 (2016).
[92] L. Lindfors, S. Forssén, J. Westergren, U. Olsson. *J. Colloid Interface Sci.* **325**, 404 (2008).
[93] A. E. Posey, K. M. Ruff, T. S. Harmon, S. L. Crick, A. Li, M. I. Diamond, R. V. Pappu. *J. Biol. Chem.* **293**, 3734 (2018).
[94] J. Wyman, S. J. Gill. *Proc. Natl. Acad. Sci. USA* **77**, 5239 (1980).
[95] K. H. Ziller, H. Rupprecht. *Drug Dev. Ind. Pharm.* **14**, 2341 (1988).
[96] A. F. Wallace, L. O. Hedges, A. Fernandez-Martinez, P. Raiteri, J. D. Gale, G. A. Waychunas, S. Whitelam, J. F. Banfield, J. J. De Yoreo. *Science* **341**, 885 (2013).
[97] M. P. Hughes, M. R. Sawaya, D. R. Boyer, L. Goldschmidt, J. A. Rodriguez, D. Cascio, L. Chong, T. Gonen, D. S. Eisenberg. *Science* **359**, 698 (2018).
[98] S. Qamar, G. Wang, S. J. Randle, F. S. Ruggeri, J. A. Varela, J. Q. Lin, E. C. Phillips, A. Miyashita, D. Williams, F. Ströhl, W. Meadows, R. Ferry, V. J. Dardov, G. G. Tartaglia, L. A. Farrer, G. S. Kaminski Schierle, C. F. Kaminski, C. E. Holt, P. E. Fraser, G. Schmitt-Ulms, D. Klenerman, T. Knowles, M. Vendruscolo, P. St GeorgeHyslop. *Cell* **173**, 720 (2018).
[99] F. T. Chan, G. S. Kaminski Schierle, J. R. Kumita, C. W. Bertoncini, C. M. Dobson, C. F. Kaminski. *Analyst* **138**, 2156 (2013).